2019

A New Generation of Magnetorheological Vehicle Suspension System With Tunable Stiffness and Damping Characteristics

Shuaishuai Sun
University of Wollongong, ssun@uow.edu.au

Xin Tang
University of Wollongong, xt955@uowmail.edu.au

Jian Yang
University of Science and Technology of China, yangj@uow.edu.au

Donghong Ning
University of Wollongong, dning@uow.edu.au

Haiping Du
University of Wollongong, hdu@uow.edu.au

See next page for additional authors

A New Generation of Magnetorheological Vehicle Suspension System With Tunable Stiffness and Damping Characteristics

Abstract

As the concept of variable stiffness (VS) and variable damping (VD) has increasingly drawn attention because of its superiority on reducing unwanted vibrations, dampers with property of varying stiffness and damping have been an attractive method to further improve vehicle performance and driver comfort. This paper presents the design, prototyping, modeling, and experimental evaluation of a VS and VD magnetorheological (MR) vehicle suspension system. It was first characterized by an INSTRON machine. Then, a phenomenological model was proposed to capture the characteristics of the damper and TS fuzzy approach was used to model the quarter car system where the proposed damper was installed. Different controllers, including skyhook, short-time Fourier transform and state observer based controller were designed to control the damper. Experimental results demonstrate that the quarter car system with the VS and VD suspension performs best in terms of reducing the sprung mass accelerations comparing with other suspensions.

Disciplines

Engineering | Science and Technology Studies

Publication Details

Sun, S., Tang, X., Yang, J., Ning, D., Du, H., Zhang, S. & Li, W. (2019). A New Generation of Magnetorheological Vehicle Suspension System With Tunable Stiffness and Damping Characteristics. IEEE Transactions on Industrial Informatics, 15 (8), 4696-4708.

Authors

Shuaishuai Sun, Xin Tang, Jian Yang, Donghong Ning, Haiping Du, Shiwu Zhang, and Weihua Li

This article has been accepted for publication in a future issue of this journal, but has not been fully edited. Content may change prior to final publication. Citation information: DOI 10.1109/TII.2018.2890290, IEEE Transactions on Industrial Informatics

A new generation of magnetorheological vehicle suspension system with tunable stiffness and damping characteristics

Shuaishuai Sun, Xin Tang, Jian Yang, Donghong Ning, Haiping Du, *Member, IEEE*, Shiwu Zhang, and Weihua Li, *Member, IEEE,*

***Abstract*— As the concept of variable stiffness and damping has drawn increasingly attention because of its superiority on reducing unwanted vibrations, dampers with property of varying stiffness and damping have been an attractive method to further improve vehicle performance and driver comfort. This paper presents the design, prototyping, modelling and experimental evaluation of a variable stiffness and variable damping (VSVD) magnetorheological (MR) vehicle suspension system. It was firstly characterized by an INSTRON machine. Then a phenomenological model was proposed to capture the characteristics of the damper and TS fuzzy approach was used to model the quarter car system where the proposed damper was installed. Different controllers, including skyhook, Short-time Fourier transform (STFT) and state observer based controller were designed to control the damper. Experimental results demonstrate that the quarter car system with the variable stiffness and damping suspension performs best in terms of reducing the sprung mass accelerations comparing with other suspensions.**

***Index Terms*—variable stiffness and damping; magnetorheological; vehicle suspension; vibration control**

I. INTRODUCTION

ACTIVE and semi-active control are two typical methods used to improve system performance [1-3]. Despite that active control performs better at reducing vibrations, the disadvantages of potential instability, complex control algorithm requirement, and large power consumption limit its common use. Therefore, researchers show increasing interest to semi-active control because of its requirements for less power and cheaper hardware but comparable performance with active system [4-7]. The application of magnetorheological fluids (MRFs) to develop semi-active control systems is a typical case. MR fluids are a kind of typical controllable fluids which can change from a free flowing viscous fluid into a semi-solid under the operation of a magnetic field, i.e. its mechanical properties (damping) will increase or decrease in response to the variations of the magnetic field. Other advantages of MR fluids is that it only needs a low voltage source to be energized and that it is much safer because of its fail-safe nature. These advantages have enabled the semi-active device with MR fluids a better option for the practical application. MR fluids based damper uses the unique characteristics of MR fluids to provide simple, quiet, and rapid-response interfaces between the electronic controls and the mechanical systems, which makes it an ideal option for vehicle suspensions. Up to date, MRF dampers have been widely implemented into vehicle suspensions to improve the vibration isolation performance [8-10]. For example, Yao et al did pioneer research on applying MR technology on vehicle suspension and developed a skyhook control strategy to control the MR vehicle suspension system [8]. MagneRide technology, proposed by Delphi Corporation, was designed based on the mechanical property of MRF and it has been used by GM Corp. on many of their Cadillac models since 2002. Choi's group conducted research on developing MR suspension systems as well as advanced controllers for them. They reported an adaptive fuzzy controller by combining the advantages of H∞ control and sliding model control in [9]. The enhanced performance under the new controller is verified numerically and experimentally. Yu's group has conducted the road testing of a vehicle mounted with four MR dampers [10] and its performance was compared with a passive suspension.

Apart from the suspension damping, the stiffness is another important component that affects the performance of a suspension. To date, passive spring has been widely used in vehicle suspension. However, passive stiffness cannot satisfy the conflict requirement of improved both ride comfort and ride stability. An idealized suspension spring is supposed to be controllable so as to provide different stiffness values depending on the specific driving and road conditions. Specifically, hard stiffness is required to guarantee the ride stability and soft stiffness is required for the ride comfort. In addition, stiffness variation can avoid suspension resonance by tuning the natural frequency of the vehicle suspension, which the suspension with only variable damping cannot achieve.

This research is supported by ARC Linkage Grants (LP160100132, No. 150100040).

S. Sun, X. Tang and W. Li are with School of Mechanical, Materials and Mechatronic Engineering, University of Wollongong, Wollongong, NSW. 2522, Australia (email: ssun@uow.edu.au; xt955@uowmail.edu.au; weihuali@uow.edu.au).

D. Ning and H. Du are with the School of Electrical, Computer and Telecommunications Engineering, University of Wollongong, Wollongong, 2522, NSW, Australia (email: hdu@uow.edu.au; dn654@uow.edu.au)

S. Zhang and J. Yang, is with Department of Precision Machinery and Precision Instrumentation, University of Science and Technology of China, Hefei, China (email: swzhang@ustc.edu.cn; jy937@ustc.edu.cn).

Corresponding Authors: W. Li and S. Zhang.

This article has been accepted for publication in a future issue of this journal, but has not been fully edited. Content may change prior to final publication. Citation information: DOI 10.1109/TII.2018.2890290, IEEE Transactions on Industrial Informatics

Based on these motivations, the concept of variable stiffness has been integrated into damping variable suspension system to form a variable stiffness and damping suspension and this topic has been attracting increasing attentions recently [11-16]. Zhang et al. [17, 18] developed a variable stiffness and damping MR device that contains an air spring, separate films, an MR valve and an accumulator. The dynamic response obtained from experiments showed that the stiffness and damping can be adjusted over a relatively large range. Following this research, Sun et al. investigated a suspension system for railway vehicles. This suspension system includes an MRF based variable stiffness air spring and an MR damper. This research theoretically verified that the variable stiffness and damping suspension has better effectiveness on suppressing vibrations than suspensions with only variable damping or variable stiffness [19]. Zhu et al. proposed a variable stiffness and damping isolator by connecting the pneumatic spring and the MR damper [20]. In this compact design, the MR damper varies the damping of the isolator while the pneumatic spring gives the isolator the variable stiffness capability. Moreover, different working modes can be switched between the passive mode and the active mode using the pneumatic spring. Raja et al. developed another variable stiffness and damping device: an MR fluid damper–liquid spring suspension system for heavy off-road vehicles [21]. Liu et al. proposed a structure with two Voigt elements (each one consisting of a constant spring and a controllable damper) in order to achieve the variable stiffness and damping [22]. In their design, the damping and the stiffness cannot be controlled independently because that the two MR dampers were installed in series. In order to improve the design, Liu and his group then proposed a new structure which could vary its stiffness and damping independently [23]. A vibration testing experiment was carried out to evaluate how it performed to isolate vibrations. The results showed that the suspension with variable stiffness and damping performed the best. Despite of the verification of the superiority of the variable stiffness and damping system, compact devices capable of varying both stiffness and damping for practical applications have rarely been developed. Based on this motivation, our group has developed a small scaled compact variable stiffness and damping shock absorber for vehicles [24-26]. However, the damping variation of the scaled device is limited. Following up our previous work, this paper developed a full scaled MR suspension system with tunable stiffness and damping characteristics and the damping variation range has been significantly improved. Furthermore, a proper control algorithm for the advanced suspension system has been developed and the effectiveness of the suspension system on vibration control has been verified on a quart car system. The structure of this paper is as follows. In Section II, the detailed design, working principle and prototype of the damper were presented. Section III presented the INSTRON testing results. Section IV illustrated the modelling for the MR damper and the quarter car test rig. Appropriate controllers were also designed in this Section. Section V presented the evaluation of the MR damper on a quart car test rig. Lastly, the conclusions were drawn in Section VI.

II. Design and working principle of the VSVD MR suspension

Figure 1 shows the structure and the prototype picture of the proposed variable stiffness and damping MR device. This device mainly consists of two damping cylinders (a bottom MR cylinder and a top MR cylinder) and two springs (spring 1 and spring 2) with different stiffness. It can be seen that the piston rod runs through both the bottom and top MR cylinders. The electromagnetic coils in these two cylinders extend generally coaxially around the piston. In addition to that, the two cylinders consist of seals and reservoirs filled with MRF. The damping force (or the damping) of the bottom cylinder is controlled by the magnetic field generated by I_d on the basis of MRF properties. Likewise, the top damping force or damping is controlled by I_s.

The working principles of the new device can be demonstrated by three different connection modes shown in Figure 2. The damping (C_1) is represented by the bottom damping which is adjusted only by the current I_d. C_1 increases as the current (I_d) increases.

The variable stiffness mechanism is controlled by current I_s. When I_s is very small, the working mechanism can be represented by mode 1 in Figure 2. Under this mode, a small damping force will be produced by the top MR damper and thus relative motion between the piston rod and the top cylinder will happen and spring k_1 will deform. In this case, spring k_1 and spring k_2 work in series. Therefore, the overall stiffness of the damper is soft.

For the second connection mode where the top damping is bigger, the deformation of the spring k_1 is restricted because of the limitation on the relative motion between the piston rod and the top cylinder, but the spring k_2 deforms more compared with the first working mode. This means that the overall stiffness of the damper is harder than the first scenario. For the last scenario (mode 3), when the top damping force is large enough to block the relative motion between the piston rod and the top cylinder, spring k_1 will produce no deformation and only spring k_2 works in response to the external force. In this case the overall stiffness of the damper reaches the maximum. Based on the above analysis, the determination of connection mode depends on the amount of the input current I_s.

The properties of stiffness variability and damping variability were tested separately using the INSTRON machine. The experimental setup is shown in Figure 3. A sinusoidal wave with a single frequency of 0.5 Hz and an amplitude of 20 mm was chosen to excite the system. To obtain the performance of stiffness variability, the applied current to the top damping cylinder was varied from 0A to 0.4A with a step of 0.2A. The applied current to the bottom damping cylinder was set as 0A in order to avoid the influence of damping. On the other hand, the current applied to the bottom damping cylinder was set to 0A, 0.5A, and 1A, respectively,

This article has been accepted for publication in a future issue of this journal, but has not been fully edited. Content may change prior to final publication. Citation information: DOI 10.1109/TII.2018.2890290, IEEE Transactions on Industrial Informatics

with the I_s maintained as 0.2A to demonstrate the performance of variable damping.

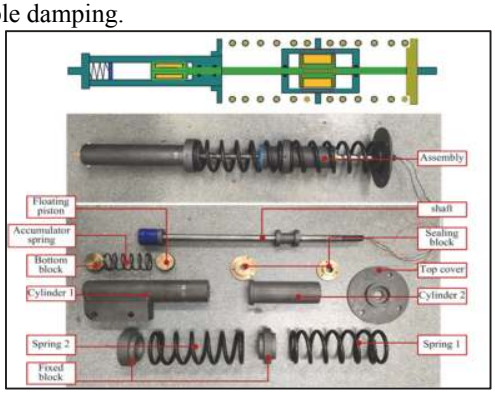

Fig.1. Design and photograph of the MR damper system with two springs.

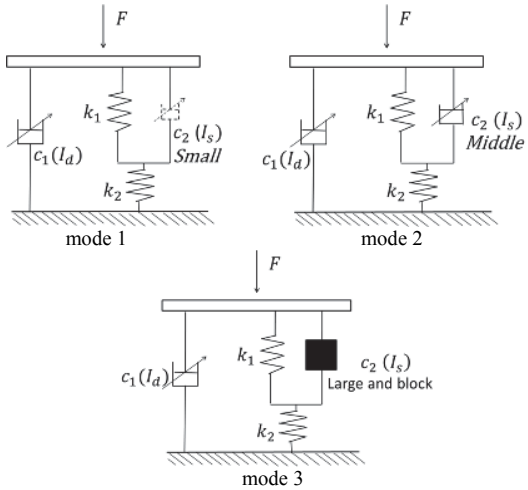

Fig.2. Schematic Diagram of Connection Mode.

III. Experimental Characterization of the Advanced MR Damper

Fig.3. Testing system with INSTRON.

Figure 4(a) shows a series of stable force-displacement loops in terms of stiffness variability and Figure 4(b) shows the corresponding force-velocity relationships. The effective stiffness of each force-displacement loop is represented by finding the slope of the straight line that intersects the end points of each force-displacement hysteresis loop, and the calculated effective stiffness is tabulated in Table 1. It is seen that the effective stiffness increases from 25.4 kN/mm to 45.2 kN/mm when the current increases from 0A to 0.4A.

Table I Effective stiffness versus I_s

I_s	0A	0.2A	0.4A
Effective stiffness (kN/m)	25.4	37.3	45.2

Table II Equivalent damping versus I_d

I_d	0A	0.5A	1A
Equivalent damping (kN·s/ m)	5.80	11.22	17.85

Figure 5 shows the variable damping characteristic including force-displacement loops (Figure 5(a)) and force-velocity loops (Figure 5(b)) under different currents of I_d (0A, 0.5 A, and 1A). It is seen that the enclosed area of the force-displacement loops increases with the increase of current I_d. As the enclosed area presents the equivalent damping, it can be concluded that the increasing I_d leads to the increase in the equivalent damping of the MR damper. The calculated equivalent damping shown in Table 2 also demonstrates this changing tendency with a variation range from 5.8KN·s/m to 17.85 kN·s/ m.

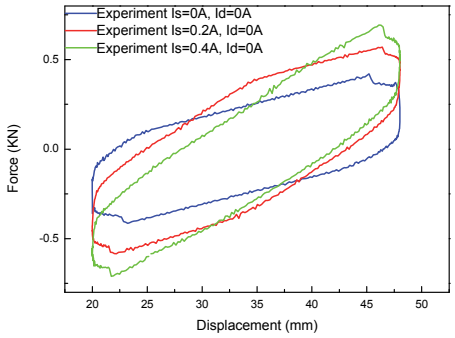

(a)

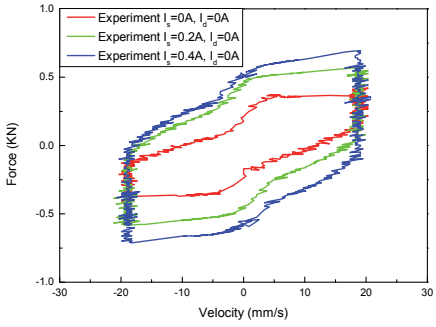

(b)

Fig. 4. Characterization of variable stiffness: (a) force – displacement relationships; (b) force-velocity relationships.

This article has been accepted for publication in a future issue of this journal, but has not been fully edited. Content may change prior to final publication. Citation information: DOI 10.1109/TII.2018.2890290, IEEE Transactions on Industrial Informatics

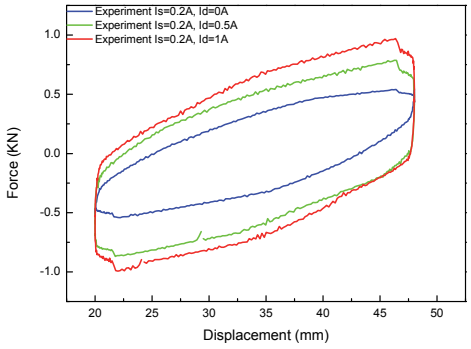

(a)

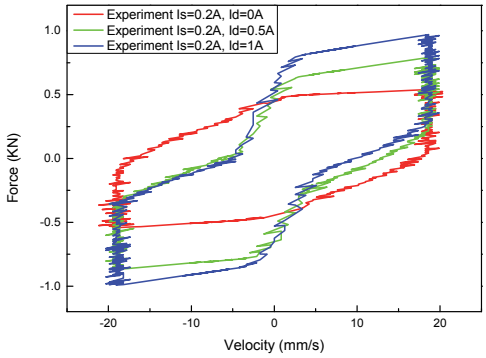

(b)

Fig. 5. Characterization of variable damping: (a) force-displacement relationships; (b) force-velocity relationships.

After the stiffness and damping variation evaluation, the response time of the MR device was also tested. As the MR damping cylinders in the stiffness controlling component and damping controlling component are the same, their response time will be the same. Thus this paper only tested the response time of the low MR damping cylinder (c_1) as a representative. In this test, the MR damper was extended under a constant speed by the INSTRON machine. During the extension, an 1A current was applied to the damper (c_1) at around 0.7s and then was removed at around 3s, as shown in Figure 6. According to Figure 6 it can be seen that the response time of the MR device is 43~44ms which is quick enough for real time control.

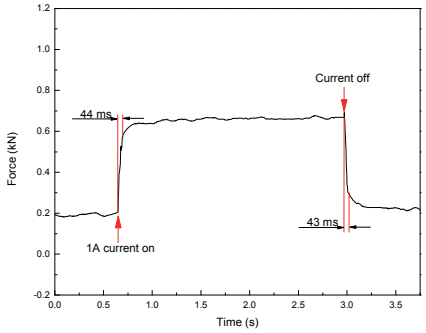

Fig. 6 Response time of the VSVD MR suspension system.

IV. Modelling of the MR Damper, a Quarter Car System and Controller Design

For the purpose of developing a controller for the VSVD MR suspension system, accurate models for the damper itself as well as the quarter car system are necessary. In this section, a phenomenological model was proposed. Then a quarter car system with this new damper was also modelled using the TS fuzzy approach. An observer was designed to estimate the velocity of the pavement input so that the real time frequency information can be obtained. Finally, a control algorithm is developed on the basis of the quarter car model and the state observer.

A. Phenomenological model for the VSVD MR device

The Bouc-Wen model has been widely accepted in describing MR behavior for its mathematical simplicity and accuracy [27, 28]. For this reason, the model proposed in this paper has incorporated the classic Bouc-Wen component, attempting to use its accuracy to describe the nonlinear characteristics and the hysteretic behavior of an MR damper. Figure 7 shows the schematic diagram of the proposed phenomenological model. It is seen that two Bouc-Wen components were used. And they are described by the evolutionary variable z_{d1}, z_{d2}, respectively, which represent a function of the time history of the displacement. The mathematical description for this model is as follows:

$$
\begin{aligned}
&F = F_{\mathrm{d}} + k_{\mathrm{s1}}(z - z_{\mathrm{k}}) + F_s \\
&F_{\mathrm{d}} = \alpha_1 z_{\mathrm{d1}} + k_{01} \cdot z + C_{01} \cdot \dot{z} \\
&F_s = \alpha_2 z_{\mathrm{d2}} + k_{02} \cdot (z - z_{\mathrm{k}}) + C_{02} \cdot (\dot{z} - \dot{z_{\mathrm{k}}}) \\
&m_{\mathrm{k}} \cdot \ddot{z_{\mathrm{k}}} + k_{\mathrm{s1}}(z_{\mathrm{k}} - z) + k_{\mathrm{s2}} \cdot z_{\mathrm{k}} = F_{\mathrm{s}}
\end{aligned}
\tag{1}
$$

where

$$
\begin{aligned}
&\dot{z_{\mathrm{d1}}} = -r_1|\dot{z}| \cdot z_{\mathrm{d1}}|z_{\mathrm{d1}}| - \beta_1 \cdot \dot{z}{z_{\mathrm{d1}}}^2 + A_{\mathrm{d1}}(\dot{z}) \\
&\dot{z_{\mathrm{d2}}} = -r_2|\dot{z} - \dot{z_{\mathrm{k}}}| \cdot z_{\mathrm{d2}}|z_{\mathrm{d2}}| - \beta_2 \cdot (\dot{z} - \dot{z_{\mathrm{k}}}){z_{\mathrm{d2}}}^2 + \\
&\qquad A_{\mathrm{d2}}(\dot{z} - \dot{z_{\mathrm{k}}}) \\
&\alpha_1 = \alpha_{1\mathrm{a}} + \alpha_{1\mathrm{b}} \cdot I_1, \;\; C_{01} = C_{01\mathrm{a}} + C_{01\mathrm{b}} \cdot I_1 \\
&\alpha_2 = \alpha_{2\mathrm{a}} + \alpha_{2\mathrm{b}} \cdot I_2, \;\; C_{02} = C_{02\mathrm{a}} + C_{02\mathrm{b}} \cdot I_2
\end{aligned}
$$

m_k is the mass of the top cylinder of the damper, A_{d1}, A_{d2}, β_1, β_2, $r_1$and r_2 are used to describe the hysteresis behaviour; α_1 and α_2 are the evolutionary coefficient; $\alpha_{1\mathrm{a}}$, $\alpha_{1\mathrm{b}}$, $\alpha_{2\mathrm{a}}$, $\alpha_{2\mathrm{b}}$, $C_{01\mathrm{a}}$, $C_{01\mathrm{b}}$, $C_{02\mathrm{a}}$, and $C_{02\mathrm{b}}$ are the constants to be determined. C_{01} and $C_{02}$are the viscous damping ;k_{s1}, k_{s2}, k_{01} , and k_{02} are the stiffness.

To model the time delay of the MR damper, a first-order filter is applied:

$$
\begin{aligned}
&\dot{I_1} = \eta(I_1 - I_{\mathrm{d}}) \\
&\dot{I_2} = \eta(I_2 - I_{\mathrm{s}})
\end{aligned}
$$

where I_{d} and I_{s} are the command currents sent to the power amplifier while I_1 and I_2 represent the real-time currents through damping cylinder c_1 and damping cylinder c_2 , respectively. The η reflects the response time of the MR damper; the larger η is the faster the damper responses. The value η is identified as -51 according to the time delay of the MR damper shown in Fig. 6.

This article has been accepted for publication in a future issue of this journal, but has not been fully edited. Content may change prior to final publication. Citation information: DOI 10.1109/TII.2018.2890290, IEEE Transactions on Industrial Informatics

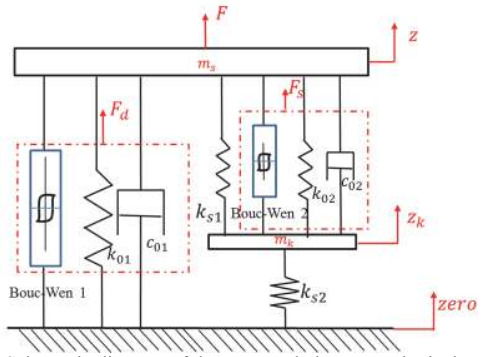

Fig. 7. Schematic diagram of the proposed phenomenological model.

To evaluate the accuracy of the proposed model in describing the damper performances, numerical simulation was conducted to identify the optimal parameters for the model to fit the experimental data shown in Figure 4 and Figure 5. A least-square method in combination with the Trust-region-reflective algorithm available in MATLAB was used to determine the parameters in this model. Table III lists the identified values for these parameters. Figure 8 shows the fitting results for the stiffness variability and the damping variability. It can be seen that the predicted hysteresis loops match well with the experimentally obtained data. This means that the proposed phenomenological model is able to predict the behaviors of the variable stiffness and damping MR device in high accuracy.

TABLE III
IDENTIFIED VALUES FOR THE PARAMETERS

Parameters	Identified values	Parameters	Identified values
A_{d1}	120	A_{d2}	89
β_1	237602	β_2	266259
r_1	219872	r_2	1277656
α_{1a}	7211	α_{1b}	23415
α_{2a}	18654	α_{2b}	43876
C_{01a}	15036	C_{01b}	11221
C_{02a}	20657	C_{02b}	1876
k_{01}	347	k_{02}	29032
k_{s1}	29976	k_{s2}	38500

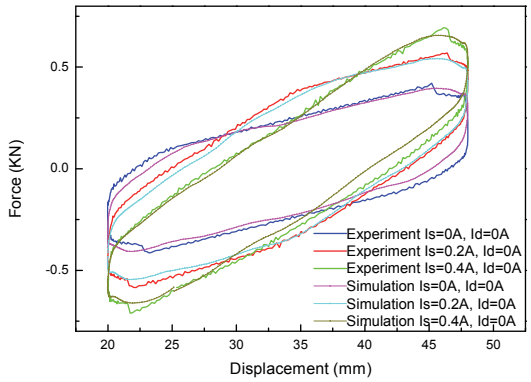

(a)

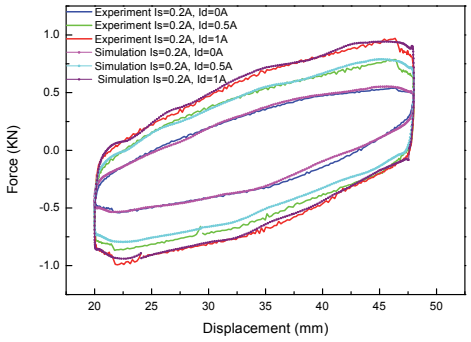

(b)

Fig. 8. Fitting results: (a) Fitting results of stiffness variability between the predicted and experimental responses; (b) Fitting results of damping variability between the predicted and experimental responses.

B. *Quarter car model with the VSVD MR device*

A quarter car model with this VSVD MR device installed was built and shown in Figure 9. Equation (3) describes the whole system:

$$\begin{aligned} m_s \cdot \ddot{z}_s + F_d + F_s + k_{s1}(z_s - z_k) &= 0 \\ m_u \cdot \ddot{z}_u - F_d + k_{s2}(z_u - z_k) + k_t(z_u - z_r) &= 0 \\ m_k \cdot \ddot{z}_k - F_s + k_{s1}(z_k - z_s) + k_{s2}(z_k - z_u) &= 0 \end{aligned} \quad (2)$$

Substitute equation (1) into equation (3), then we can obtain:

$$\begin{aligned} m_s \cdot \ddot{z}_s = &-[(\alpha_{1a} + \alpha_{1b} \cdot I_1) \cdot z_{d1} + k_{01}(z_s - z_u) + \\ &(c_{01a} + c_{01b} \cdot I_1)(\dot{z}_s - \dot{z}_u) + k_{s1}(z_s - z_k) + \\ &(\alpha_{2a} + \alpha_{2b} \cdot I_2) \cdot z_{d2} + k_{02}(z_s - z_k) + \\ &(c_{02a} + c_{02b} \cdot I_2)(\dot{z}_s - \dot{z}_k)] \\ m_u \cdot \ddot{z}_u = &(\alpha_{1a} + \alpha_{1b} \cdot I_1) \cdot z_{d1} + k_{01}(z_s - z_u) \\ &+(c_{01a} + c_{01b} \cdot I_1)(\dot{z}_s - \dot{z}_u) + k_{s2}(z_k - z_u) \\ &-k_t(z_u - z_r) \\ m_k \cdot \ddot{z}_k = &k_{s1}(z_s - z_k) + (\alpha_{2a} + \alpha_{2b} \cdot I_2) \\ &\cdot z_{d2} + k_{02}(z_s - z_k) + (c_{02a} + c_{02b} \cdot I_2)(\dot{z}_s - \\ &\dot{z}_k) - k_{s2}(z_k - z_u) \end{aligned}$$

where $m_s$is the sprung mass, $m_u$is the unsprung mass, m_k is the mass of the top cylinder of the damper, z_s is the displacement of the sprung mass, $z_u$is the displacement of the unsprung mass, z_k is the displacement of the top damper cylinder.

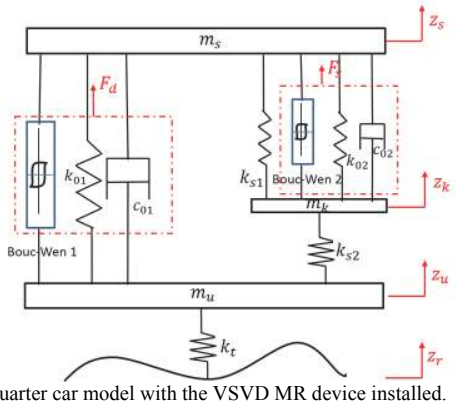

Fig. 9 Quarter car model with the VSVD MR device installed.

This article has been accepted for publication in a future issue of this journal, but has not been fully edited. Content may change prior to final publication. Citation information: DOI 10.1109/TII.2018.2890290, IEEE Transactions on Industrial Informatics

In order to build a state-space for the quarter car system, define $\widetilde{f_1}$, $\widetilde{f_2}$as:

$$\widetilde{f_1} = -r_1|\dot{z}_\mathrm{s} - \dot{z}_\mathrm{u}| \cdot z_{\mathrm{d}1}|z_{\mathrm{d}1}| - \beta_1(\dot{z}_\mathrm{s} - \dot{z}_\mathrm{u})|z_{\mathrm{d}1}|^2 \quad (3)$$
$$\widetilde{f_2} = -r_2|\dot{z}_\mathrm{s} - \dot{z}_\mathrm{k}| \cdot z_{\mathrm{d}2}|z_{\mathrm{d}2}| - \beta_2(\dot{z}_\mathrm{s} - \dot{z}_\mathrm{k})|z_{\mathrm{d}2}|^2$$

Define the state variables as follows:

$$x_1 = \dot{z}_\mathrm{s};\ x_2 = \dot{z}_\mathrm{u};\ x_3 = \dot{z}_\mathrm{k};\ x_4 = z_\mathrm{s} - z_\mathrm{k};\ x_5 = z_\mathrm{k} - z_\mathrm{u};\ x_6 = z_\mathrm{u} - z_\mathrm{r};\ x_7 = z_{\mathrm{d}1};\ x_8 = z_{\mathrm{d}2} \quad (4)$$

and the state vector as:

$$\boldsymbol{x} = [x_1\ x_2\ x_3\ x_4\ x_5\ x_6\ x_7\ x_8]^\mathrm{T} \quad (5)$$

then define: $f_1 = \frac{\widetilde{f_1}}{x_7}$, $f_2 = \frac{\widetilde{f_2}}{x_8}$,

$$f_3 = \alpha_{1\mathrm{b}} \cdot x_7 + c_{01\mathrm{b}}(x_1 - x_2) \quad (6)$$
$$f_4 = \alpha_{2\mathrm{b}} \cdot x_8 + c_{02\mathrm{b}}(x_1 - x_3)$$

Then (3) can be written as:

$$\begin{aligned} m_\mathrm{s} \cdot \dot{x_1} = -[&\alpha_{1\mathrm{a}} \cdot x_7 + k_{01} \cdot x_4 + c_{01\mathrm{a}}x_1 - c_{01\mathrm{a}}x_2 + f_3 I_1 \\ &+k_{\mathrm{s}1}x_4 - k_{\mathrm{s}1}x_5 + \alpha_{2\mathrm{a}} \cdot x_8 + k_{02}x_4 - k_{02}x_5 + c_{02\mathrm{a}} \\ &\cdot x_1 - c_{02\mathrm{a}} \cdot x_3 + f_4 \cdot I_2] \end{aligned}$$
$$m_\mathrm{u} \cdot \dot{x_2} = \alpha_{1\mathrm{a}} \cdot x_7 + k_{01} \cdot x_4 + c_{01\mathrm{a}}x_1 - c_{01\mathrm{a}}x_2 + k_{\mathrm{s}2}x_5 - k_\mathrm{t}x_6 + f_3 \cdot I_1$$
$$m_\mathrm{k} \cdot \dot{x_3} = k_{\mathrm{s}1}x_4 - k_{\mathrm{s}1}x_5 + \alpha_{2\mathrm{a}} \cdot x_8 + k_{02}x_4 - k_{02}x_5 + c_{02\mathrm{a}} \cdot x_1 - c_{02\mathrm{a}} \cdot x_3 - k_{\mathrm{s}2}x_5 + f_4 \cdot I_2$$
$$\dot{x_4} = x_1 - x_2 \quad (7)$$
$$\dot{x_5} = x_3 - x_2$$
$$\dot{x_6} = x_2 - \dot{z_\mathrm{r}}$$
$$\dot{x_7} = f_1 x_7 + A_{\mathrm{d}1}(x_1 - x_2)$$
$$\dot{x_8} = f_2 x_8 + A_{\mathrm{d}2}(x_1 - x_3)$$

We can write a state-space for system (4) as:

$$\dot{\boldsymbol{x}}(t) = \boldsymbol{A}\boldsymbol{x} + \boldsymbol{B}_1 w + \boldsymbol{B}_2 \boldsymbol{u} \quad (8)$$

where

$$\boldsymbol{A} = \begin{bmatrix} \frac{c_{01\mathrm{a}} + c_{02\mathrm{a}}}{-m_\mathrm{s}} & \frac{-c_{01\mathrm{a}}}{-m_\mathrm{s}} & \frac{-c_{02\mathrm{a}}}{-m_\mathrm{s}} & \frac{k_{01} + k_{\mathrm{s}1} + k_{02}}{-m_\mathrm{s}} \\ \frac{c_{01\mathrm{a}}}{m_\mathrm{u}} & \frac{-c_{01\mathrm{a}}}{m_\mathrm{u}} & \frac{0}{m_\mathrm{u}} & \frac{k_{01}}{m_\mathrm{u}} \\ \frac{c_{02\mathrm{a}}}{m_\mathrm{k}} & \frac{0}{m_\mathrm{k}} & \frac{-c_{02\mathrm{a}}}{m_\mathrm{k}} & \frac{k_{\mathrm{s}1} + k_{02}}{m_\mathrm{k}} \\ 1 & -1 & 0 & 0 \\ 0 & -1 & 1 & 0 \\ 0 & 1 & 0 & 0 \\ A_{\mathrm{d}1} & -A_{\mathrm{d}1} & 0 & 0 \\ A_{\mathrm{d}2} & 0 & A_{\mathrm{d}2} & 0 \end{bmatrix}$$

$$\begin{bmatrix} \frac{-k_{\mathrm{s}1} - k_{02}}{-m_\mathrm{s}} & \frac{0}{m_\mathrm{u}} & \frac{\alpha_{1\mathrm{a}}}{-m_\mathrm{s}} & \frac{\alpha_{2\mathrm{a}}}{-m_\mathrm{s}} \\ \frac{k_{\mathrm{s}2}}{m_\mathrm{u}} & \frac{-k_\mathrm{t}}{m_\mathrm{u}} & \frac{\alpha_{1\mathrm{a}}}{m_\mathrm{u}} & \frac{0}{m_\mathrm{u}} \\ \frac{-k_{\mathrm{s}1} - k_{02} - k_{\mathrm{s}2}}{m_\mathrm{k}} & \frac{0}{m_\mathrm{k}} & \frac{0}{m_\mathrm{k}} & \frac{\alpha_{2\mathrm{a}}}{-m_\mathrm{k}} \\ 0 & 0 & 0 & 0 \\ 0 & 0 & 0 & 0 \\ 0 & 0 & 0 & 0 \\ 0 & 0 & f_1 & 0 \\ 0 & 0 & 0 & f_2 \end{bmatrix}$$

$$\boldsymbol{B}_1 = [0 \quad 0 \quad 0 \quad 0 \quad 0 \quad -1 \quad 0 \quad 0]^T$$

$$\boldsymbol{B}_2 = \begin{bmatrix} \frac{f_3}{-m_\mathrm{s}} & \frac{f_4}{-m_\mathrm{s}} \\ \frac{f_3}{m_\mathrm{u}} & \frac{0}{m_\mathrm{u}} \\ \frac{0}{m_\mathrm{k}} & \frac{f_4}{m_\mathrm{k}} \\ 0 & 0 \\ 0 & 0 \\ 0 & 0 \\ 0 & 0 \\ 0 & 0 \end{bmatrix}$$

$$w = z_\mathrm{r}$$

$$\mathbf{u} = \begin{bmatrix} I_1 \\ I_2 \end{bmatrix}$$

C. *TS Fuzzy* modeling *of the quarter car with variable stiffness and damping characteristics*

Considering that the state variables x_1, x_2, x_7, and x_8 are actually limited in practice for a stable system, the nonlinear f_1 ,f_2, f_3, and f_4 should also be bounded in operation. We represent f_1 ,f_2, f_3, and f_4 using their minimum values and maximum values following "sector nonlinearity" approach [29]:

$$\begin{aligned} f_1 &= M_1 \cdot f_{1\max} + M_2 \cdot f_{1\min}, \\ f_2 &= N_1 \cdot f_{2\max} + N_2 \cdot f_{2\min}, \\ f_3 &= T_1 \cdot f_{3\max} + T_2 \cdot f_{3\min}, \\ f_4 &= H_1 \cdot f_{4\max} + H_2 \cdot f_{4\min}, \end{aligned} \quad (9)$$

where $f_{(i)\max}$ $(i = 1,2,3,4)$ represents the maximum values and $f_{(i)\min}$ $(i = 1,2,3,4)$ is the minimum values of the nonlinear $f_{(i)}$ $(i = 1,2,3,4)$. $M_{(i)}$, $N_{(i)}$, $T_{(i)}$, and $H_{(i)}$ $(i = 1,2)$ are fuzzy membership functions and satisfy:

$$\begin{aligned} M_1 + M_2 &= 1 \\ N_1 + N_2 &= 1 \\ T_1 + T_2 &= 1 \\ H_1 + H_2 &= 1 \end{aligned} \quad (10)$$

And the member functions are defined as:

$$\begin{aligned} M_1 &= \frac{f_1 - f_{1\min}}{f_{1\max} - f_{1\min}}, & M_2 &= \frac{f_{2\max} - f_2}{f_{2\max} - f_{2\min}}, \\ N_1 &= \frac{f_2 - f_{2\min}}{f_{2\max} - f_{2\min}}, & N_2 &= \frac{f_{2\max} - f_2}{f_{2\max} - f_{2\min}}, \\ T_1 &= \frac{f_3 - f_{3\min}}{f_{3\max} - f_{3\min}}, & T_2 &= \frac{f_{3\max} - f_3}{f_{3\max} - f_{3\min}} \\ H_1 &= \frac{f_4 - f_{4\min}}{f_{4\max} - f_{4\min}}, & H_2 &= \frac{f_{4\max} - f_4}{f_{4\max} - f_{4\min}} \end{aligned} \quad (11)$$

Then the nonlinear quarter car system can be described by the abovementioned linear subsystems. For each possibility, there is a corresponding state–space equation:

If $f_1 = M_1, f_2 = N_1, f_3 = T_1, f_4 = H_1,$
Then $\dot{\boldsymbol{x}} = \boldsymbol{A}_{(1)}\boldsymbol{x} + \boldsymbol{B}_1 w + \boldsymbol{B}_{2(1)}u$
If $f_1 = M_1, f_2 = N_1, f_3 = T_1, f_4 = H_2,$
Then $\dot{\boldsymbol{x}} = \boldsymbol{A}_{(2)}\boldsymbol{x} + \boldsymbol{B}_1 w + \boldsymbol{B}_{2(2)}u$
If $f_1 = M_1, f_2 = N_1, f_3 = T_2, f_4 = H_1,$

This article has been accepted for publication in a future issue of this journal, but has not been fully edited. Content may change prior to final publication. Citation information: DOI 10.1109/TII.2018.2890290, IEEE Transactions on Industrial Informatics

Then $\dot{\boldsymbol{x}} = \boldsymbol{A}_{(3)}\boldsymbol{x} + \boldsymbol{B}_1 w + \boldsymbol{B}_{2(3)}u$

If $f_1 = M_1, f_2 = N_1, f_3 = T_2, f_4 = H_2$,
Then $\dot{\boldsymbol{x}} = \boldsymbol{A}_{(4)}\boldsymbol{x} + \boldsymbol{B}_1 w + \boldsymbol{B}_{2(4)}u$

If $f_1 = M_1, f_2 = N_2, f_3 = T_1, f_4 = H_1$,
Then $\dot{\boldsymbol{x}} = \boldsymbol{A}_{(5)}\boldsymbol{x} + \boldsymbol{B}_1 w + \boldsymbol{B}_{2(5)}u$

If $f_1 = M_1, f_2 = N_2, f_3 = T_2, f_4 = H_1$,
Then $\dot{\boldsymbol{x}} = \boldsymbol{A}_{(6)}\boldsymbol{x} + \boldsymbol{B}_1 w + \boldsymbol{B}_{2(6)}u$

If $f_1 = M_1, f_2 = N_2, f_3 = T_2, f_4 = H_2$,
Then $\dot{\boldsymbol{x}} = \boldsymbol{A}_{(7)}\boldsymbol{x} + \boldsymbol{B}_1 w + \boldsymbol{B}_{2(7)}u$

If $f_1 = M_2, f_2 = N_1, f_3 = T_1, f_4 = H_1$,
Then $\dot{\boldsymbol{x}} = \boldsymbol{A}_{(8)}\boldsymbol{x} + \boldsymbol{B}_1 w + \boldsymbol{B}_{2(8)}u$

If $f_1 = M_2, f_2 = N_2, f_3 = T_1, f_4 = H_1$,
Then $\dot{\boldsymbol{x}} = \boldsymbol{A}_{(9)}\boldsymbol{x} + \boldsymbol{B}_1 w + \boldsymbol{B}_{2(9)}u$

If $f_1 = M_2, f_2 = N_2, f_3 = T_2, f_4 = H_1$,
Then $\dot{\boldsymbol{x}} = \boldsymbol{A}_{(10)}\boldsymbol{x} + \boldsymbol{B}_1 w + \boldsymbol{B}_{2(10)}u$

If $f_1 = M_2, f_2 = N_2, f_3 = T_2, f_4 = H_2$,
Then $\dot{\boldsymbol{x}} = \boldsymbol{A}_{(11)}\boldsymbol{x} + \boldsymbol{B}_1 w + \boldsymbol{B}_{2(11)}u$

If $f_1 = M_1, f_2 = N_2, f_3 = T_1, f_4 = H_2$,
Then $\dot{\boldsymbol{x}} = \boldsymbol{A}_{(12)}\boldsymbol{x} + \boldsymbol{B}_1 w + \boldsymbol{B}_{2(12)}u$

If $f_1 = M_2, f_2 = N_1, f_3 = T_1, f_4 = H_2$,
Then $\dot{\boldsymbol{x}} = \boldsymbol{A}_{(13)}\boldsymbol{x} + \boldsymbol{B}_1 w + \boldsymbol{B}_{2(13)}u$

If $f_1 = M_2, f_2 = N_1, f_3 = T_2, f_4 = H_1$,
Then $\dot{\boldsymbol{x}} = \boldsymbol{A}_{(14)}\boldsymbol{x} + \boldsymbol{B}_1 w + \boldsymbol{B}_{2(14)}u$

If $f_1 = M_2, f_2 = N_1, f_3 = T_2, f_4 = H_2$,
Then $\dot{\boldsymbol{x}} = \boldsymbol{A}_{(15)}\boldsymbol{x} + \boldsymbol{B}_1 w + \boldsymbol{B}_{2(15)}u$

If $f_1 = M_2, f_2 = N_2, f_3 = T_1, f_4 = H_2$,
Then $\dot{\boldsymbol{x}} = \boldsymbol{A}_{(16)}\boldsymbol{x} + \boldsymbol{B}_1 w + \boldsymbol{B}_{2(16)}u$

where $\boldsymbol{A}_{(i)}$ $(i = 1,2,3,\ldots,16)$ are obtained by replacing $f_{(i)}$ $(i = 1,2)$ in matrix $\boldsymbol{A}$ of (8) with $f_{(i)\max}$ and $f_{(i)\min}$, respectively.

Then the TS fuzzy model for the nonlinear quarter car under the bounded state variables is obtained as:

$$\dot{\boldsymbol{x}} = \sum_{i=1}^{16} h_i\left[\boldsymbol{A}_{(i)}\boldsymbol{x} + \boldsymbol{B}_1 w + \boldsymbol{B}_{2(i)}\dot{u}\right] = \boldsymbol{A}_{\mathrm{h}}\boldsymbol{x} + \boldsymbol{B}_1 w + \boldsymbol{B}_{2\mathrm{h}}\dot{u} \quad (12)$$

where $\boldsymbol{A}_{\mathrm{h}} = \sum_{i=1}^{16} h_i A_{(i)}$ $\boldsymbol{B}_{2\mathrm{h}} = \sum_{i=1}^{16} h_i B_{2(i)}$

$h_1 = M_1N_1T_1H_1$, $h_2 = M_1N_1T_1H_2$
$h_3 = M_1N_1T_2H_1$, $h_4 = M_1N_1T_2H_2$
$h_5 = M_1N_2T_1H_1$, $h_6 = M_1N_2T_2H_1$
$h_7 = M_1N_2T_2H_2$, $h_8 = M_2N_1T_1H_1$
$h_9 = M_2N_2T_1H_1$, $h_{10} = M_2N_2T_2H_1$
$h_{11} = M_2N_2T_2H_2$, $h_{12} = M_1N_2T_1H_2$
$h_{13} = M_2N_1T_1H_2$, $h_{14} = M_2N_1T_2H_1$
$h_{15} = M_2N_1T_2H_2$, $h_{16} = M_2N_2T_1H_2$

And $h_{(i)}$ $(i = 1,2,3,\ldots,16)$ satisfy: $\sum_{i=1}^{16} h_i = 1$

D. Controller design for the variable stiffness and damping suspension.

As the stiffness and the damping of the damper are separately adjusted and controlled, two different controllers have to be designed. For the variable damping, we chose the classic skyhook controller which is simple while effective. The description for skyhook controller is:

$$\boldsymbol{F}_{\mathrm{sky}} = \begin{cases} C_{\max}\dot{z}_{\mathrm{s}}, & \dot{z}_{\mathrm{s}}(\dot{z}_{\mathrm{s}} - \dot{z}_{\mathrm{u}}) \geq 0 \\ C_{\min}\dot{z}_{\mathrm{s}}, & \dot{z}_{\mathrm{s}}(\dot{z}_{\mathrm{s}} - \dot{z}_{\mathrm{u}}) < 0 \end{cases} \quad (13)$$

where $C_{\max}$ and $C_{\min}$ are the maximum and minimum skyhook gains, which correspond to the command voltages $I_{\max}$ and $I_{\min}$, respectively. In this experiment, the specific skyhook force is expressed as the MR damper force with the control output voltage, $I_{\max}$=0.8A and $I_{\min} = 0$A.

In terms of the control strategy for the stiffness component, it is to avoid the resonance of the quarter car under a pavement input. As the stiffness is controlled according to the dominant excitation frequency, the real time frequency information of the pavement input is very important in determining the stiffness. At the same time, ideal switching frequencies, where the high stiffness should be switched to the low stiffness or vice versa, should also be obtained as a reference for the real time frequency. In addition, the stroke limitation should be taken into consideration to protect the damper from any collision.

Determining the switching frequency is to guarantee that an optimal or minimal transmissibility (ratio of the quarter car response to the excitation signal) can be obtained. For example, the simulation result shown in Figure 10 in terms of the transmissibility from the excitation z_{r} to the sprung mass acceleration $\ddot{z}_{\mathrm{s}}$, the switching frequency is 1.51Hz and the desired minimum transmissibility is composed of the black segment which is indicated as high stiffness before the 1.51Hz and the red segment indicated as low stiffness after 1.51Hz. According to the simulation results, the switching frequency is related to the damping force (F_{d}). As the damping force F_{d} is controlled by current I_{d}, the switching frequency is a function of I_{d}. Table IV gives the corresponding relationship between the switching frequency and I_{d}. It can be calculated that the relationship between the switching frequency and the current is linear, therefore, the switching frequency can be defined as linear function of the applied current:

$$f_{\mathrm{c}} = -0.15 * I_{\mathrm{d}} + 1.50 \quad (14)$$

Real time dominant frequency of the pavement input is needed to compare with the above obtained switching frequency. Then the stiffness will be determined according to their relationship. To measure the real time dominant frequency, we have to firstly collect the velocity data ($\dot{z}_{\mathrm{r}}$) of the pavement input. Then the dominant frequency information of the pavement input will be obtained by analyzing the velocity using STFT. As $\dot{z}_{\mathrm{r}}$ is immeasurable in practice, we designed an observer to estimate the information. The design of the observer is based on the TS fuzzy model built in section IV. C. The observer is designed as follow:

Define the measurable suspension deflection as:

$$\boldsymbol{y} = [z_{\mathrm{s}} - z_{\mathrm{u}}] \quad (15)$$

and its state-space equation is : $\boldsymbol{y} = \boldsymbol{C} \cdot \boldsymbol{x}$

then $\boldsymbol{C} = [0\ 0\ 0\ 0\ 1\ 0\ 0\ 0]$

Then define the proposed observer as:

$$\dot{\hat{\boldsymbol{x}}} = \boldsymbol{A}_{\boldsymbol{h}}\hat{\boldsymbol{x}} + \boldsymbol{L}_{\mathrm{h}}(\boldsymbol{y} - \hat{\boldsymbol{y}}) + \boldsymbol{B}_{2\mathrm{h}} \cdot \boldsymbol{u} \quad (16)$$
$$\hat{\boldsymbol{y}} = \boldsymbol{C}\hat{\boldsymbol{x}}$$

where $\hat{\boldsymbol{x}}$ is the observer state vector, $\hat{\boldsymbol{y}}$ is the estimated output, L_{h} is the observer gain matrix to be designed. Considering (8)

This article has been accepted for publication in a future issue of this journal, but has not been fully edited. Content may change prior to final publication. Citation information: DOI 10.1109/TII.2018.2890290, IEEE Transactions on Industrial Informatics

and (16), the error dynamics model is defined as:

$$\begin{aligned}\dot{\boldsymbol{e}} &= \dot{\boldsymbol{x}} - \dot{\hat{\boldsymbol{x}}} \\ &= \boldsymbol{A}_{\mathrm{h}}\boldsymbol{x} + \boldsymbol{B}_1 w + \boldsymbol{B}_{2\mathrm{h}} u - \boldsymbol{A}_{\mathrm{h}}\hat{\boldsymbol{x}} - \boldsymbol{L}_{\mathrm{h}} y + \boldsymbol{L}_{\mathrm{h}}\hat{\boldsymbol{y}} - \boldsymbol{B}_{2\mathrm{h}} u \\ &= \boldsymbol{A}_{\mathrm{h}}(\boldsymbol{x} - \hat{\boldsymbol{x}}) - \boldsymbol{L}_{\mathbf{h}}(\boldsymbol{y} - \hat{\boldsymbol{y}}) + \boldsymbol{B}_1 w \\ &= \boldsymbol{A}_{\mathrm{h}} \cdot e - \boldsymbol{L}_{\mathrm{h}} \cdot \mathrm{C} \cdot \boldsymbol{e} + \boldsymbol{B}_1 w \\ &= (\boldsymbol{A}_{\mathrm{h}} - \boldsymbol{L}_{\mathrm{h}} \cdot \mathrm{C}) \cdot \boldsymbol{e} + \boldsymbol{B}_1 w \end{aligned} \quad (17)$$

where $\boldsymbol{e} = \boldsymbol{x} - \hat{\boldsymbol{x}}$ is the estimated error.

Suppose that $\boldsymbol{A}_{\mathrm{oh}} = (\boldsymbol{A}_{\mathrm{h}} - \boldsymbol{L}_{\mathrm{h}}) \cdot \mathbf{C}$

Then $\dot{\boldsymbol{e}} = \boldsymbol{A}_{\mathrm{oh}} \cdot \boldsymbol{e} + \boldsymbol{B}_1 w$ (18)

By defining an objective output as:

$\boldsymbol{z}_0 = \boldsymbol{e} = \boldsymbol{x} - \hat{\boldsymbol{x}} = \boldsymbol{E}_0 \cdot \boldsymbol{e}$ (19)

where $\boldsymbol{E}_0 = 1$.

Then if there exists a matrix P>0 such that the following LMI is satisfied:

$$\begin{bmatrix} \boldsymbol{P}\boldsymbol{A}_{\mathrm{oh}} + \boldsymbol{A}_{\mathrm{oh}}^{\mathrm{T}} & \boldsymbol{P}\boldsymbol{B}_1 & \boldsymbol{E}_0^{\mathrm{T}} \\ * & -r_0^2\boldsymbol{I} & 0 \\ * & * & -\boldsymbol{I} \end{bmatrix} < 0 \quad (20)$$

Then the system (8) is stable with $H\infty$ disturbance attenuation $r_0 > 0$. Using the definition $\boldsymbol{Y} = \boldsymbol{P}\boldsymbol{L}_{\mathrm{h}}$ and solving the LMI, the observer gain matrix can be obtained as $\boldsymbol{L}_{\mathrm{h}} = \boldsymbol{P}^{-1}\boldsymbol{Y}$. Then the observer is successfully designed.

TABLE IV
CORRESPONDENCE BETWEEN THE SWITCHING FREQUENCY AND THE APPLIED CURRENT

Damper current I_d(A)	Switching frequency (Hz)
0.0	1.50
0.1	1.49
0.2	1.47
0.3	1.46
0.4	1.45
0.5	1.43
0.6	1.41
0.7	1.40
0.8	1.38

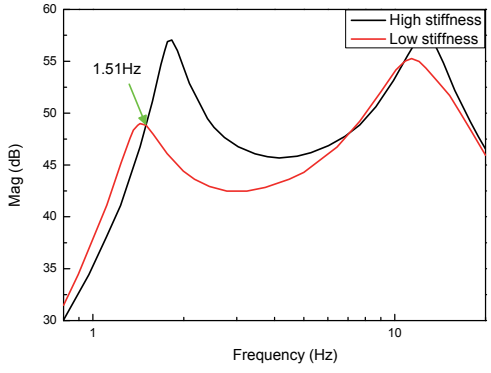

Fig.10. Example of the switching frequency

Apart from the switching frequency, the determination of the stiffness also depends on the stoke limitation. Once the suspension deflection is not less than the stoke limitation, the maximum stiffness will be turned on to avoid any collision. This value guarantees that the deformation of spring slows down before any collision under the maximum stoke limitation. Therefore, the controller to determine the stiffness is:

$$k_{\mathrm{s}} = \begin{cases} k_{\max}(I_{\mathrm{s}} = 0.4A)\,, & f_{\mathrm{req}} < f_{\mathrm{c}}\ OR\ |z_{\mathrm{s}} - z_{\mathrm{u}}| \geq s_{\mathrm{t}}, \\ k_{\min}(I_{\mathrm{s}} = 0\mathrm{A})\,, & \text{Otherwise.} \end{cases} \quad (20)$$

where f_{c} is the switching frequency, f_{req} is the real time dominant frequency of the pavement input signal.

V. EFFECTIVENESS EVALUATION AND ANALYSIS OF THE DAMPER ON A QUART CAR TEST RIG

In this section, the proposed TS fuzzy modelling and controller were applied to control the VSVD MR suspension system which is installed on a real quarter car test rig.

Figure 11 shows the experimental setup of the quarter car test rig. The tire is excited by a vertical road profile generated by a hydraulic system manufactured by the CRAM Corporation. The hydraulic actuator is controlled by the real-time control board (Model: myRio-1900, NI Corp.) with a proportional-integral-derivative (PID) controller. Specifically, as the first step, a target road profile was set in the controller and the real time road profile generated by the hydraulic system will be measured by a laser displacement sensor labelled as No. 9 in Figure 11 (Model: LB-11, Keyence Corp.). A PID controller is designed to control the real time road profile to trace the target road profile. Then a close-loop control is built to generate different target road profiles.

Regarding the VSVD MR suspension controlling, two displacement input signals, the suspension deflection (SD) and the sprung mass displacement (SMD), are measured by the two laser sensors (Model: LB-11, Keyence Corp.); the acceleration input signal, the sprung mass acceleration, is measured by an accelerometer (Model: ADXL327, Analog Devices Corp.). By running the VSVD control algorithm based on these inputs, the real-time control board calculates the command currents, I_{d} and I_{s}, and sends them to the power amplifiers. After amplifying the power of the signals, the currents considered as the system outputs will be sent to the two MR dampers. Furthermore, the tire deflection can be calculated by using the signals from the laser sensors and will be used to indicate the road holding performance of different suspensions. The sprung mass acceleration will be used to measure the ride comfort of suspensions. A force sensor (Interface: SSM-AJ-20KN) is installed in between the MR damper system and the sprung mass to measure the force generated by the damper system under different control cases. As comparison, the other two suspensions are also tested, i.e. passive suspension where conventional passive damper (original damper from Toyota vehicle) was used; variable damping (VD) suspension where the variable stiffness and damping shock absorber was used but the stiffness was fixed by setting the applied current I_{s} as 0.35A.

For the convenience of the reader, Figure 11 shows the control flowchart of the system. It can be seen that the measureable variables, z_{s} and $z_{\mathrm{s}} - z_{\mathrm{u}}$, are transmitted to the skyhook variable damping (VD) controller and thus the desired damping can be determined. As for the variable stiffness (VS)

This article has been accepted for publication in a future issue of this journal, but has not been fully edited. Content may change prior to final publication. Citation information: DOI 10.1109/TII.2018.2890290, IEEE Transactions on Industrial Informatics

controller, it needs three inputs and produces one output. One of the inputs, $\dot{z}_r$, needs to be estimated by the observer designed in the above section as this variable is immeasurable in practice. After the estimation of $\dot{z}_r$, a frequency estimator will calculate the real time dominant frequency of the excitation using the Short-time Fourier Transform [30]. I_d provides the information of the switching frequency according to (14) and the suspension deflection $(z_s - z_u)$ will be compared with the damper stoke limitation. Then the VS controller can determine the desired stiffness of the MR damper.

Two excitation signals were used to evaluate the whole system: bump road profile and random road profile. These two excitations are generated by the equation (21) and equation (22), which are classic road profile generation method [31-32]. The expression for the bump excitation is:

$$z_r(t) = \begin{cases} \frac{a}{2}\left(1 - \cos\left(\frac{2\pi V_0}{l}t\right)\right), & 0 \le t \le \frac{l}{V_0} \\ 0, & t > \frac{l}{V_0} \end{cases} \quad (21)$$

where V_0 is the vehicle speed, a and l are the height and the length of the bump, In the experiment, a=30mm, l=0.8m, $V_0 = 1.39\ m/s$.

The road displacement of the random road profile is generated by:

$$\dot{z}_r(t) + \rho V_0 z_r(t) = V_0 W_n \quad (22)$$

where W_n is white noise with the intensity $2\sigma^2\rho V$, ρ is the road roughness parameter, σ^2 is the covariance of road irregularity. In this experiment, $\rho = 0.45\text{m}^{-1}$, $\sigma^2 = 300\text{mm}^2$, V_0 changes from 20 m/s to 10m/s at 15th second. After the road profiles are generated, they will be fixed and will be used to evaluate the performance of different vehicle suspensions. The same road profiles guarantee the fair comparison of different suspensions.

During the test, the first step was to install the passive suspension to the quart car test rig and evaluate its vibration isolation performance under both bump excitation and random excitation. After that, the passive suspension was replaced by the VSVD MR suspension and both VS controller and VD controller were turned on. Then the performance of the VSVD MR suspension on vibration control was evaluated. The last step was to turn off the VS controller and leave the VD controller on to make the VSVD suspension function as a pure VD suspension. Then the dynamic performance of the VD suspension system under the two road profiles was evaluated. The evaluation results are shown as follow.

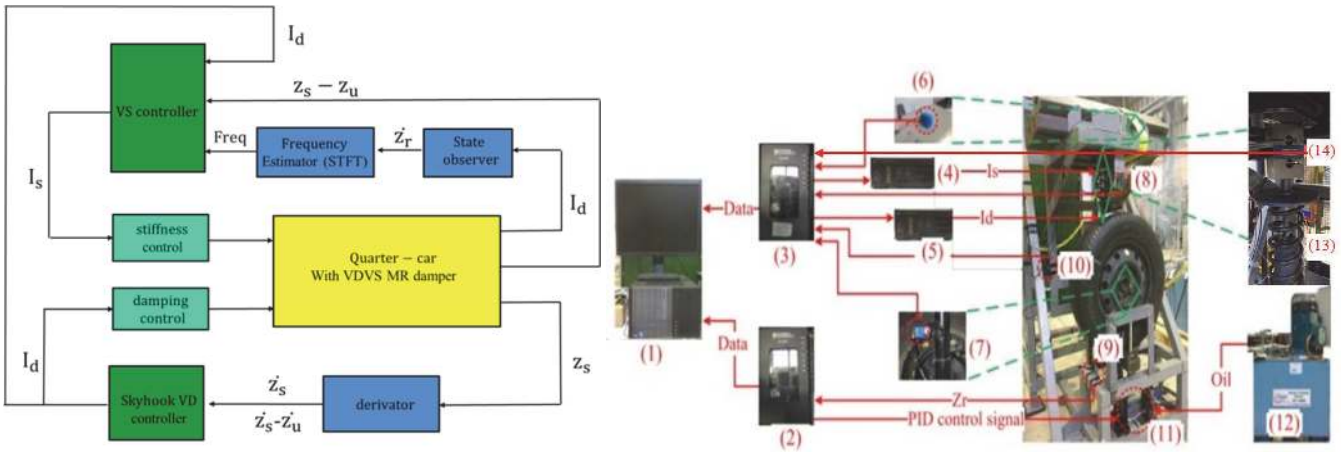

Fig.11. Control flow chart and Experimental setup: (1) computer, (2) NI real-time control board I, (3) NI real-time comtrol board II, (4, 5) power amplifier, (6) accelerometer, (7-10) laser sensors, (11) hydraulic actuator, (12) hydraulic station, (13) the proposed VSVD MR suspension system and (14) force sensor.

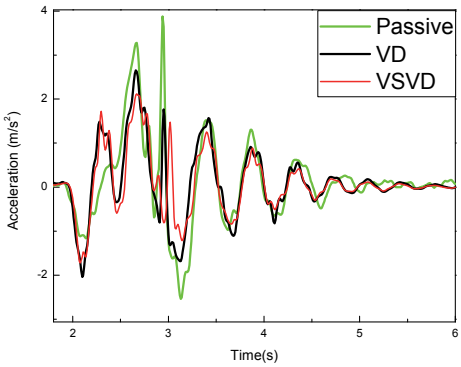

Fig. 12 Sprung mass acceleration under bump road profile in time domain.

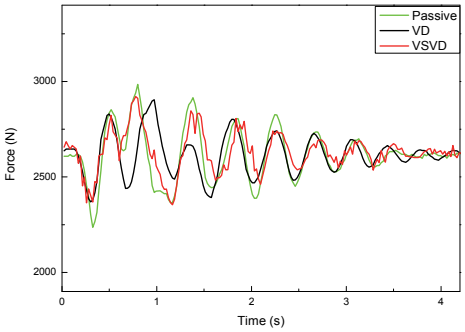

Fig. 13 The force generated by the MR damper system under bump road profile

Figure 12 and Figure 13 show the vibration reduction performance and the forces generated by the three different

This article has been accepted for publication in a future issue of this journal, but has not been fully edited. Content may change prior to final publication. Citation information: DOI 10.1109/TII.2018.2890290, IEEE Transactions on Industrial Informatics

suspension systems under the bump road profile excitation. It is seen that the VD suspension performs better than traditional passive suspension and VSVD suspension performs the best in reducing the sprung acceleration.

After the bump road evaluation, random road evaluation is further conducted. Time histories of the sprung mass acceleration of the quarter car system under random road profile are shown in Figure 14. The forces generated by different damper systems under random excitation have been presented in Figure 15 as well. In order to thoroughly evaluate the vibration reduction effectiveness of the suspension under different vehicle velocities, we conducted the evaluation under different running speeds, i.e. the vehicle velocity was changed from 20m/s to 10m/s at 15th second, as shown in Figure 14. It can be seen that the sprung mass acceleration under the passive case has the biggest peak value during the whole time history. VSVD case and VD case both perform better than the passive case. However, the sprung mass acceleration under VSVD case is further reduced than under VD case. This means that the quarter-car system performs best under the VSVD suspension where the damping and the stiffness of the damper are both controlled in real time. In order to illustrate the experimental results more clearly, the sprung mass acceleration responses under the three cases are compared in Table V and Table VI in terms of their RMS values and weighted RMS values respectively. It is seen that the acceleration RMS under VSVD case has the smallest value. And the reduction percentage compared to the passive case show that VSVD case is more effective on reducing the sprung mass acceleration than the VD case.

Figure 16 shows the frequency spectrum of the sprung mass acceleration under the random excitation with different velocity. Generally, it can be seen that the passive case performed worst and VSVD case performed best in reducing the vibration. But closer observations reveal that VD case is slightly better than VSVD control case around frequency of 1.1Hz. That is because VD control case has a high fixed stiffness which results in lower transmissibility in low frequency range. To sum up, the experimental results have shown the superiority of the proposed MR suspension system over the passive system and the variable damping system in terms of enhancing the ride comfort.

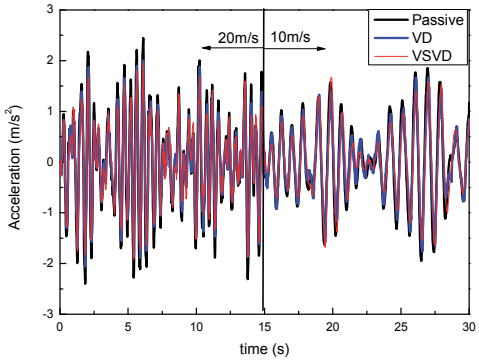

Fig.14. Sprung mass acceleration under random excitation in time domain.

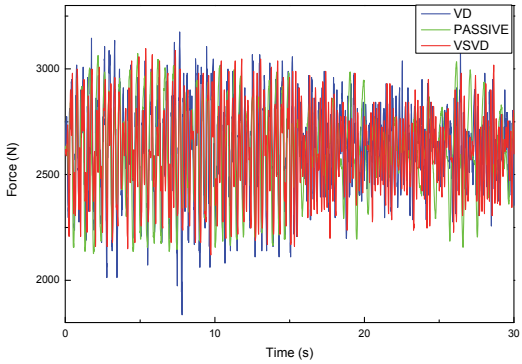

Fig. 15 The force generated by the MR damper system under random road profile

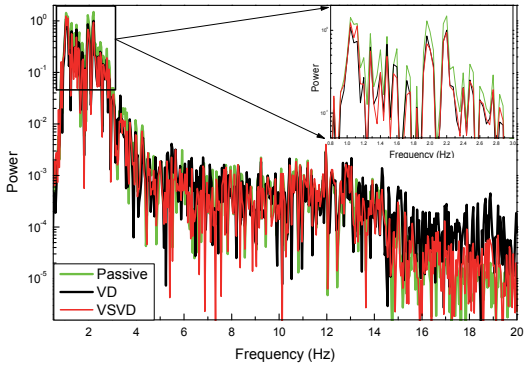

Fig.16. Sprung mass acceleration in frequency domain.

TABLE V
AVERAGE ACCELERATION RMS VALUE

Variable	Passive	VSVD	VD
RMS (m/s^2)	0.97	0.76	0.79
Reduction percentage (%)	NA	-21.6	-18.6

TABLE VI
WEIGHTED ACCELERATION RMS VALUE

Variable	Passive	VSVD	VD
RMS (m/s^2)	0.7319	0.598	0.6175
Reduction percentage (%)	NA	-18.3	-15.6

As the road holding performance is very important for vehicle driving, the road holding performance of the three different suspension systems under a sinusoidal signal with sweeping frequency from 0Hz to 20Hz was also evaluated. The tire deflection and the damper-generated force are both collected and presented in Figure 17 and Figure 18, respectively. It can be seen that the tire deflection of the VD suspension is slightly larger than the other two and the VSVD suspension and passive suspension have comparable tire deflection. This means that the VSVD suspension system can improve the ride comfort of a vehicle without deteriorating its road holding performance, which is desirable for vehicle driving.

This article has been accepted for publication in a future issue of this journal, but has not been fully edited. Content may change prior to final publication. Citation information: DOI 10.1109/TII.2018.2890290, IEEE Transactions on Industrial Informatics

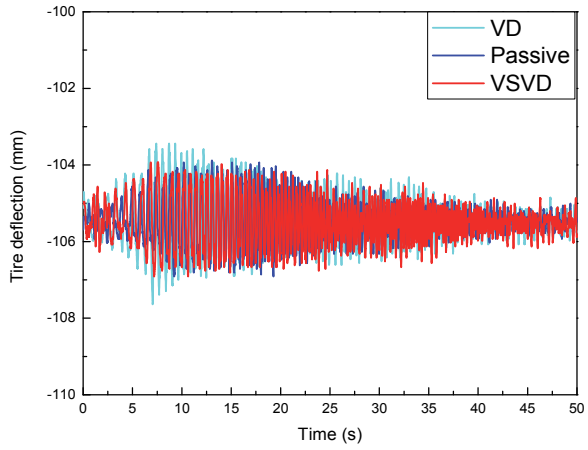

Fig. 17 Tire deflection under sweeping excitation.

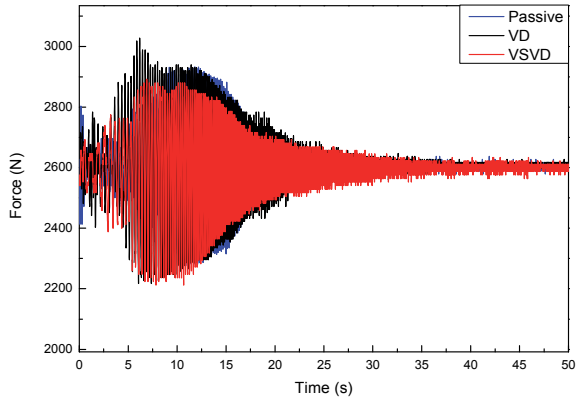

Fig. 18 The force generated by the MR damper system under sweep road profile

VI. CONCLUSION

An MR damper with tunable stiffness and damping characteristics was successfully designed in this study. The testing results by an INSTRON machine verified its feasibility to change both the stiffness and damping in response to the magnetic field variations. The stiffness and damping of the damper show clear increase when the applied current increase, respectively. The proposed phenomenological model was capable of predicting the stiffness and damping variation characteristics of the advanced MR damper. A control algorithm on the basis of STFT, skyhook and a state observer is built to control the advanced MR damper and a quarter car test rig is built to evaluate the performance of the MR suspension system on vibration control. Experimental tests were conducted under bump and random excitation. The results show that the VSVD MR suspension system with tunable stiffness and damping performs better in improving the ride comfort comparing to the passive suspension system and VD suspension system.

I. REFERENCES

[1] D. Ning, S. Sun, H. Li, H. Du, W. Li, “Active control of an innovative seat suspension system with acceleration measurement based friction estimation”, Journal of Sound and Vibration, vol. 384, pp. 28-44, 2016.

[2] W. He, Y. Ouyang, and J. Hong, “Vibration control of a flexible robotic manipulator in the presence of input deadzone”, IEEE Transactions on Industrial Informatics, vol.13, pp. 48-59, 2017.

[3] C. Yang, Y. Jiang, Z. Li, W. He, C. Su, “Neural control of bimanual robots with guaranteed global stability and motion precision”, IEEE Transactions on Industrial Informatics, online first, 2017.

[4] H. O'Neill and G. Wale, "Semi-active suspension improves rail vehicle ride," Computing & Control Engineering Journal, vol. 5, pp. 183-188, 1994.

[5] J. Tang, "Passive and semi-active airspring suspensions for rail passenger vehicles—theory and practice," Proceedings of the Institution of Mechanical Engineers, Part F: Journal of Rail and Rapid Transit, vol. 210, pp. 103-117, 1996.

[6] J. Li, D. Wang, J. Duan, H. He, Y. Xia, W. Zhu, "Structural design and control of a small-MRF damper under 50 N soft-landing applications", IEEE Transactions on Industrial Informatics, vol. 11, pp. 612-619, 2015.

[7] A. Stribersky, A. Kienberger, G. Wagner, and H. Müller, "Design and evaluation of a semi-active damping system for rail vehicles," Vehicle System Dynamics, vol. 29, pp. 669-681, 1998.

[8] G. Yao, F. Yap, G. Chen, W. H. Li, and S. Yeo, “MR damper and its application for semi-active control of vehicle suspension system,” Mechatronics, vol. 12, no. 7, pp. 963-973, 2002.

[9] D. K. Shin and S.-B. Choi, “Design of a new adaptive fuzzy controller and its application to vibration control of a vehicle seat installed with an MR damper,” Smart Materials and Structures, vol. 24, no. 8, pp. 85012–85031, 2015.

[10] M. Yu, C. Liao, W. Chen, and S. Huang, “Study on MR semi-active suspension system and its road testing,” Journal of Intelligent Material Systems and Structures, vol. 17, no. 8-9, pp. 801-806, 2006.

[11] S. Sun, H. Deng, and W. Li, "A variable stiffness and damping suspension system for trains," in SPIE Smart Structures and Materials+ Nondestructive Evaluation and Health Monitoring, 2014, pp. 90570P-90570P-12.

[12] G. Y. Pan and F. Q. Fan, "Research on semi-active suspension system with variable stiffness and damping," in Applied Mechanics and Materials, 2012, pp. 584-589.

[13] H. P. Gavin and N. S. Doke, "Resonance suppression through variable stiffness and damping mechanisms," in 1999 Symposium on Smart Structures and Materials, 1999, pp. 43-53.

[14] K. K. Walsh, K. D. Grupenhof, K. L. Little, A. Martin, and C. A. Moore Jr, "Development and testing of a newly proposed continuously variable stiffness/damping device for vibration control," in SPIE Smart Structures and Materials+ Nondestructive Evaluation and Health Monitoring, 2012, pp. 83452N-83452N-16.

[15] F. Zhou, P. Tan, W. Yan, and L. Wei, "Theoretical and experimental research on a new system of semi-active structural control with variable stiffness and damping," Earthquake Engineering and Engineering Vibration, vol. 1, pp. 130-135, 2002.

[16] G. Liao, X. Gong, S. Xuan, C. Kang, and L. Zong, "Development of a real-time tunable stiffness and damping vibration isolator based on magnetorheological elastomer," Journal of Intelligent Material Systems and Structures, vol. 23, pp. 25-33, 2012.

[17] X. Zhang, X. Wang, W. Li, and K. Kostidis, "Variable stiffness and damping MR isolator," in Journal of Physics: Conference Series, 2009, Art no. 012088.

[18] W. Li, X. Wang, X. Zhang, and Y. Zhou, "Development and analysis of a variable stiffness damper using an MR bladder," Smart materials and structures, vol. 18, Art no. 074007, 2009.

[19] S. Sun, H. Deng, and W. Li, "A variable stiffness and damping suspension system for trains," in SPIE Smart Structures and Materials+ Nondestructive Evaluation and Health Monitoring, 2014, pp. 90570P-90570P-12.

[20] X. Zhu, X. Jing, and L. Cheng, "A magnetorheological fluid embedded pneumatic vibration isolator allowing independently adjustable stiffness and damping," Smart Materials and Structures, vol. 20, Art no. 085025, 2011.

[21] P. Raja, X. Wang, and F. Gordaninejad, "A high-force controllable MR fluid damper–liquid spring suspension system," Smart Materials and Structures, vol. 23, Art no. 015021, 2014.

[22] Y. Liu, H. Matsuhisa, H. Utsuno, and J. G. Park, "Vibration isolation by a variable stiffness and damping system," JSME International Journal Series C, vol. 48, pp. 305-310, 2005.

This article has been accepted for publication in a future issue of this journal, but has not been fully edited. Content may change prior to final publication. Citation information: DOI 10.1109/TII.2018.2890290, IEEE Transactions on Industrial Informatics

[23] Y. Liu, H. Matsuhisa, and H. Utsuno, "Semi-active vibration isolation system with variable stiffness and damping control," Journal of sound and vibration, vol. 313, pp. 16-28, 2008.

[24] S. S. Sun, H. X. Deng, H. Du, W. H. Li, J. Yang, G. P. Liu, G. Alici, and T. H. Yan, "A Compact Variable Stiffness and Damping Shock Absorber for Vehicle Suspension", IEEE-ASME Transactions on Mechatronics, 20, 2621-2629, 2015.

[25] S. S. Sun, J. Yang, W. H. Li, H. Deng, H. Du, and G. Alici, "Development of a novel variable and damping magnetorheological fluid damper", Smart Materials and Structures, 24, 085021, 2015.

[26] Z. Xing, M. Yu, S. S. Sun, J. Fu, and W. H. Li, "A hybrid magnetorheological elastomer-fluid (MRE-F) isolation mount: development and experimental validation", Smart Materials and Structures, 25, 015026, 2015.

[27] D. Wang, and W. Liao, "Magnetorheological fluid dampers: a review of parametric modelling", Smart Materials and Structures, vol. 20, Art No. 023001, 2011.

[28] B. Spencer Jr, S. Dyke, M. Sain, and J. Carlson, "Phenomenological model for magnetorheological dampers," *Journal of engineering mechanics,* vol. 123, no. 3, pp. 230-238, 1997.

[29] K. Tanaka and H. O. Wang, Fuzzy Control Systems Design and Analysis: A Linear Matrix Inequality Approach, New York: Wiley, 2001.

[30] S. Sun, H. Deng, J. Yang, W. Li, H. Du, G. Alici, M. Nakano, "An adaptive tuned vibration absorber based on multilayered MR elastomers," Smart Materials and Structures, vol. 24, Art No. 045045, 2015.

[31] S.-B. Choi and W.-K. Kim, "Vibration control of a semi-active suspension featuring electrorheological fluid dampers," Journal of sound and vibration, vol. 234, pp. 537-546, 2000.

[32] H. Du, J. Lam, K. Cheung, W. Li, and N. Zhang, "Direct voltage control of magnetorheological damper for vehicle suspensions," Smart Materials and Structures, vol. 22, Art no. 105016, 2013.

Shuaishuai Sun received the B.E. degree in mechanical engineering and automation from the China University of Mining and Technology, Beijing, China, in 2011, and PhD degree from University of Wollongong, Australia in 2016. He is currently working as a research fellow at the School of Mechanical, Material, Mechatronics and Biomedical Engineering, University of Wollongong, Wollongong, N.S.W, Australia. His research interests include smart materials and structures, innovative actuators for locomotive robot, vibration control, and self-sensing self-power MR devices. He has published more than 50 journal articles in his research field.

Xin Tang received the B.E. degree in automation engineering from the University of Electronic Science and Technology of China, Chengdu, China, in 2012. He received the Ph.D. degree at the School of Mechanical, Material, Mechatronics and Biomedical, University of Wollongong in 2018. His research interests include the vibration control of semi-active vehicle suspension utilizing MR technology and roust control applications.

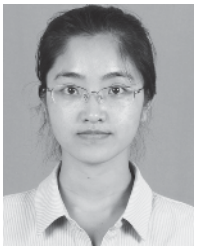

Jian Yang reveived the B.E. degree in Automation in China University of Petroleum (East), China, in 2011, and PhD degree from University of Wollongong, Australia. She is currently working as a postdoc at University of Science and Technology of China, Hefei, China. Her research mainly focuses on the application of MR techonology on the protection of building from earthquake and mechanical vibration control.

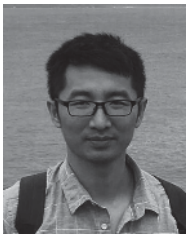

Donghong Ning received the B.E. degree in Agricultural Mechanization and Automation from College of Mechanical and Electronic Engineering, North West Agriculture and Forestry University in 2012. He recieved the Ph.D. degree at the School of Electrical, Computer and Telecommunications Engineering, University of Wollongong in 2017. His research interests include seat suspension vibration control and multi-degrees of freedom vibration control.

Haiping Du received the Ph.D. degree in mechanical design and theory from Shanghai Jiao Tong University, Shanghai, China, in 2002. He was a Research Fellow with the University of Technology, Sydney, from 2005 to 2009, and was a Postdoctoral Research Associate with Imperial College London from 2003 to 2005 and the University of Hong Kong from 2002 to 2003. He is currently a professor at the School of Electrical, Computer and Telecommunications Engineering, University of Wollongong, Wollongong, N.S.W, Australia. He is the Editorial Advisory Board Member of the Journal of Sound and Vibration. Dr. Du was an Associate Editor of the IEEE control systems Society Conference. He received the Endeavour Research Fellowship in 2012.

Shiwu Zhang received the B.S. degree in mechanical and electrical engineering, and the Ph.D. degree in precision instrumentation and precision machinery from the University of Science and Technology of China (USTC), Hefei, China, in 1997 and 2003, respectively. He is currently an Associate Professor with the Department of Precision Machinery and Precision Instrumentation, USTC. His current research interests include smart materials and their applications in bioinspired robots, amphibious robot, and terradynamics.

Weihua Li received the B.E. and M.E. degrees from the University of Science and Technology of China, Hefei, China, in 1992 and 1995, respectively, and the Ph.D degree from Nanyang Technological University, Nanyang, Singapore, in 2001. He was with the school of Mechanical and Production Engineering, Nanyang Technological University, as a Research Fellow, from 2001 to 2003. He has been with the School of Mechanical, Materials and Mechatronic Engineering, University of Wollongong, Wollongong, N.S.W, Australia, as an Academic Staff Member, since 2003. He has published more than 350 technical articles in refereed international journals and conferences. He serves as an Associate Editor or Editorial Board Member for ten international journals. Dr. Li received the number of awards, including Fellow of the Institute of Engineers Australia, Fellow of the Institute of Physics, UK, the JSPS Invitation Fellowship in 2014, the Endeavour Research Fellowship in 2011, and the Scientific Visits to China Program Awards.